This is to certify that the
thesis entitled

Theoretical and Experimental Investigation Into the Transient
Behavior of Centrifugal Pendulum Vibration Absorbers

presented by

Daniel Palmer

has been accepted towards fulfillment
of the requirements for the

M.S. degree in Mechanical Engineering

Alan Haddow

Major Professor's Signature

9/29/05

Date

THEORETICAL AND EXPERIMENTAL INVESTIGATION INTO THE TRANSIENT BEHAVIOR OF CENTRIFUGAL PENDULUM VIBRATION ABSORBERS

By

Daniel Palmer

A Thesis

Submitted to
Michigan State University
in partial fulfillment of the requirements
for the degree of

Master of Science

Department of Mechanical Engineering

2005

ABSTRACT

THEORETICAL AND EXPERIMENTAL INVESTIGATION INTO THE TRANSIENT BEHAVIOR OF CENTRIFUGAL PENDULUM VIBRATION ABSORBERS

By

Daniel Palmer

This work focuses on the dynamic behavior of a rotor with attached, circular-path, centrifugal vibration absorbers. Starting from the full non-linear equations of motion, a new non-dimensional procedure is introduced that allows the results to be applied to a wider range of applications than has previously been possible. In particular, the research has been motivated by applications in the automotive industry, and as such, an important component of the research work deals with the transient behavior of the system that results from sudden changes in the applied torque and excitation order. Tests are run on a fully instrumented experimental apparatus and the results are compared to numerical simulations and approximate analytical solutions. All comparisons are in very close agreement. Throughout the work, special attention is given to the physical interpretation of the results and, for example, parameter values are chosen to closely correspond to applications of practical importance. Related to this is a discussion of the important design parameters and the influence they have on the overall performance of a system with attached centrifugal vibration absorbers.

To my dad

ACKNOWLEDGMENTS

My greatest thanks go to my advisor, Dr. Alan Haddow, for giving me the opportunity to work on this project, and for his encouragement and guidance along the way. I want to thank Dr. Steve Shaw for all of his advice and his contributions to this work. I would also like to thank Bruce Geist for everything he has done for me. Not only for his advice, but for being responsible for the money I had to support myself over the past four months. I consider myself extremely lucky to have had the chance to work with the three of them, and I hope the quality of this work reflects my appreciation and respect.

Special thanks to the National Science Foundation for supplying the grant that helped construct the lab equipment, and to Roy Bailiff for making the modifications to lab equipment that allowed me to run my tests. Thank you to everyone who assisted me during my time at Michigan State University.

TABLE OF CONTENTS

LIST OF TABLES

LIST OF FIGURES

CHAPTER 1

Introduction

Torsional vibration is common in many dynamic systems. Typically, it is caused by a harmonically varying force, or torque. There are many ways of reducing torsional vibration, such as the use of a vibration absorber. In a linear (non-rotating) system, an absorber's natural frequency is tuned to match the frequency of the applied force. The same is true when dealing with torsional vibration absorbers, which will be discussed here. However, in such systems, the frequency of the applied torque is often related to the rotational speed itself. An example of this is an internal combustion engine where cylinder firings occur at a specific crankshaft position causing a spike in the torque. For a single cylinder 4-stroke engine, this would occur once per every other revolution of the crankshaft. In these types of systems the vibration-inducing torque is a function of position rather than time. This makes the use of centrifugal pendulum vibration absorbers (CPVAs) very appealing, since the linear natural frequency of a CPVA varies with the speed of rotation, discussed in detail in Section 2.2.

A simple example of a CPVA is a pendulum attached to a rotor. Similar to the way gravity is the restoring force in a vertically hanging pendulum, the spinning rotor creates a centrifugal restoring force on the pendulum absorber. When setup correctly, the swinging motion of the pendulum creates a counter-torque opposite to the torque applied to the rotor, reducing or eliminating the torsional vibration.

1.1 Background

Wilson [10] gives a detailed report of the early history of Pendulum Absorbers. Centrifugal Pendulum Vibration Absorbers have been used as early as the 1920s [2]. They have been used successfully in various applications, including diesel engine camshafts, high-performance race engine applications, helicopter rotors and even radial aircraft engines in WWII.

Throughout the history of CPVAs, multiple geometric configurations have been used to implement this type of dynamics. One of the earliest concepts for these types of absorbers involves liquid columns in U-shaped channels designed to affect the dynamics of rotating components. Other designs that have been utilized include a bifilar suspension design used in radial aircraft engines [4] and a roll-form absorber used in helicopter rotors [6]. Both of these are still used today in various applications.

Although a strong argument can be made in their favor, pendulum absorbers are not the only method used to reduce torsional vibration. One commonly used method is to increase the mass (inertia) of a rotating system, typically by using a flywheel. A drawback to this is that the extra mass decreases performance by requiring more effort to induce changes in motion. Another method is to increase the rotational damping. Dissipating energy through increased damping is not always the best solution as it may generate unwanted heat or noise, and the system will require an additional energy input to maintain a constant motion. There are also active vibration canceling devices that monitor vibration levels to deal with unwanted vibration. These devices can be very complex and expensive, and often only mask the unwanted vibration instead of actually removing its root cause.

CPVAs are extremely useful for reducing torsional vibrations, since little additional mass is needed and often much of the additional mass can be removed from elsewhere in the original system. For example, the counter-weight or external damper on an engine crankshaft. Little of the energy applied to the system is lost through damping, and a pendulum absorber system can be simple and cheap to incorporate into a rotating assembly.

Previous works have focused on various aspects of pendulum absorbers, including stability, modes of operation in multiple absorber systems and non-circular absorber paths [1, 3, 6, 7]. However, there are no reports on the transient behavior of CPVAs.

1.2 Purpose of This Work

A significant amount of work has already been done on pendulum absorbers, as discussed in the previous section. However, a recent topic of inquiry involving CPVAs, especially by the automotive industry, has been their transient response. The wide use of cylinder deactivation systems in internal combustion engines to conserve fuel during light-torque operation is a leading cause for this investigation. Engines are typically well-balanced for their normal operating mode, however, when the number of active cylinders are reduced, unwanted vibrations can occur. One method used to avoid this problem is to map a specific range of operation where the vibration is acceptable, and only use the reduced cylinder mode in this range. With CPVAs, the vibration could be reduced and reduced-cylinder mode could be implemented over a wider range of operating conditions, greatly improving fuel economy. The purpose of this thesis is to explore the behavior of the absorbers when the system is subject to changing torque conditions, which would be similar to an automotive engine with cylinder deactivation capabilities. The experimental results will be compared to theoretical work to check that they agree. It is important to be able to predict transient behavior to be able to utilize CPVAs in various applications where torque conditions are not constant. This work will also serve as a brief compilation of previous works on circular path absorbers.

1.3 Thesis Organization

The next chapter presents the mathematical modeling of the system to be studied and theoretical approximations along with some transformations allowing results to be applicable to a much wider range of scenarios. Chapter 3 is more practical for application. It has general information that is useful for the application of pendulum absorbers, and how results are influenced by various parameters. Chapter 4 reports on and discusses, the experimental results. Tests include step changes in applied torque to monitor the transient behavior of the system. Simulated results are also given in this chapter. The final chapter summarizes the main contributions of this work and includes recommendations for future research in this area.

CHAPTER 2

Mathematical Modeling

This chapter outlines some of the mathematical theory behind CPVAs. First, the equations of motion are derived for a simplified model of a rotor and single pendulum absorber, using Lagrange's method. The equations are then linearized to extract certain information from the system, for example, tuning. Other mathematical manipulations are done, uncluding non-dimensionalization, so that results can easily be compared from different systems.

2.1 Equations of Motion

A simple model was used to derive the equations of motion, see Figure 2.1. There is rotor with inertia J, with a single pendulum attached at a distance R from the fixed center of rotation of the rotor, point O. The pendulum is made up of an arbitrarily-shaped mass, m, with a center of gravity a distance r from its own center of rotation, point O_a. Viscous damping is also considered to be part of the model. The coefficients of the viscous damping are c_0 and c_a, for the rotor and absorber respectively. Finally, a torque, T, is applied to the rotor.

It should be noted here, that this model represents absorbers that follow circular paths as they swing. While this does limit the range of uses for the model, past re-

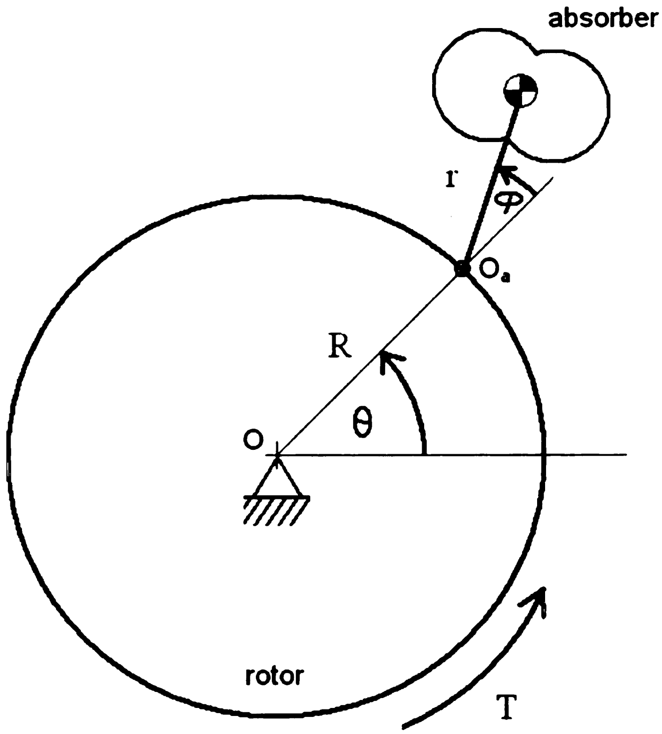

Figure 2.1. Model of rotor/absorber system

searchers such as Alsuwaiyan and Schmitz [1, 7], have derived equations for absorbers that follow general paths. However, the model used here does allow for an absorber with a distributed mass as opposed to a point mass absorber. This is an important characteristic to include, especially for practical applications.

Since the primary purpose of this thesis is to explore the transient behavior of pendulum absorbers, a single absorber model is adequate. A system with multiple absorbers will have an identical response providing there is synchronous motion of all absorbers. This is true as long as the mass of the single absorber is equivalent to the sum of the masses of the multiple absorbers, and as long as the multiple absorbers are identical in almost every way. The multiple absorbers must be tuned identically, have the same damping, and the same mass. Slight variations between absorbers can greatly influence the stability of the system in some circumstances. Alsuwaiyan and Chao [1, 3] have researched the stability and unison response of multiple absorber systems.

In order to use Lagrange's method to get the equations of motion, the energy of the system must first be calculated. It is easy to see that as long as the rotor is spinning in a horizontal plane, there is no potential energy. Note, the kinetic energy in the system can be broken into several components. From the rotor, there is a rotational energy term, of the form $\frac{1}{2}J\dot{\theta}^2$. From the absorber, there is a rotational component as well as a translational component, which are $\frac{1}{2}m\rho^2(\dot{\theta}+\dot{\phi})^2$ and $\frac{1}{2}mv_m^2$ respectively. Where v_m is the magnitude of the velocity of the absorber's center of gravity, and ρ is the radius of gyration of the absorber about its center of gravity. Equation 2.1 shows the total kinetic energy of the system.

$$K.E. = \frac{1}{2}J\dot{\theta}^2 + \frac{1}{2}m\rho^2(\dot{\theta}+\dot{\phi})^2 + \frac{1}{2}mv_m^2$$

where (2.1)

$$v_m^2 = (R^2+r^2)\dot{\theta}^2 + (2\dot{\theta}+\dot{\phi})r^2\dot{\phi} + (\dot{\theta}+\dot{\phi})2rR\dot{\theta}\cos\phi$$

Using Lagrange's method, equations for θ and ϕ can be derived

$$\begin{aligned}&\Big[J + m(R^2+r^2+\rho^2) + 2mrR\cos\phi\Big]\ddot{\theta} + m(\rho^2 + rR\cos\phi + r^2)\ddot{\phi}\\ &- 2mrR\dot{\theta}\dot{\phi}\sin\phi - mrR\dot{\phi}^2\sin\phi = T - c_0\dot{\theta}\end{aligned} \tag{2.2}$$

$$m(\rho^2+r^2)\ddot{\phi} + m(\rho^2+r^2+rR\cos\phi)\ddot{\theta} + mrR\dot{\theta}^2\sin\phi = -c_a\dot{\phi} \tag{2.3}$$

The torque applied to the rotor is assumed to be of the form

$$\begin{aligned} T &= T_0 + T_f \sin(n\theta) \\ &\approx T_0 + T_f \sin(n\Omega t) \end{aligned} \tag{2.4}$$

where Ω is the mean speed of the rotor and n is the order of excitation, for small changes about a constant mean speed.

The two forms are nearly identical, with the θ dependent version being slightly more accurate for modeling the torque in an internal combustion engine, or similar system. It is useful to be able to express the torque as either a function of rotor position, θ, or time, t, depending on the independent variable used in the equations of motion.

A torque of this form (θ dependent) is used to model torque that may actually be seen in practice. While a realistic torque would be a much more complicated signal, Equation 2.4 is meant to model the most dominant harmonic. Part of this harmonic, the order of excitation, n, is often used when refering to this type of forced vibration. In the example mentioned in the previous chapter, a single-cylinder four-stroke internal combustion engine would have an order of excitation of $\frac{1}{2}$. Since the order of excitation is often fixed for a given application, this term is useful when designing an absorber geometry. The reason for this is described in the next section.

From Equation 2.2, an expression for the counter-torque on the rotor caused by the motion of the pendulum can be derived. By separating the equation of motion for a rigid rotor with no absorbers attached,

$$J\ddot{\theta} + c_0\dot{\theta} = T$$

the the remaining terms in Equation 2.2 must be the result of the absorber. Therefore, an expression for the absorber counter-torque can be written

$$\begin{aligned} T_{counter} = & -\left[mR^2 + m(r^2+\rho^2) + 2mrR\cos\phi\right]\ddot{\theta} \\ & - m(rR\cos\phi + r^2 + \rho^2)\ddot{\phi} + mrR(2\dot{\theta}+\dot{\phi})\dot{\phi}\sin\phi \\ = & - mrR(\ddot{\theta}+\ddot{\phi})\cos\phi - mR^2\ddot{\theta} + mrR(\dot{\theta}+\dot{\phi})^2\sin\phi + c_a\dot{\phi} \end{aligned} \tag{2.5}$$

2.2 Simplifications

In order to simplify the equations of motion, certain assumptions can be made and manipulations can be used. Linearization about a fixed absorber position makes it easy to calculate the linearized natural frequency of the absorbers, used for tuning the absorber to a specific order. To get the equations into a form comparable with previous researchers, as well as a form to perform the method of averaging, a transformation of the independent variable is used. This is followed by defining some non-dimensional parameters, which are also substituted.

The first simplification that is made is shown in Equation 2.6. It is assumed that the mean component of the torque, T_0, is equal in magnitude to the torque generated from the rotor damping, c_0, when the rotor is turning at a steady speed. At slower speeds, the mean torque is greater than the rotor damping, and a net acceleration occurs until an equilibrium is reached. This equilibrium speed, or the mean speed at which the rotor turns for a given T_0 is given the symbol Ω. The mean rotor speed is used significantly in the derivations in this chapter.

$$\Omega = \frac{T_0}{c_0} \tag{2.6}$$

As mentioned in the previous section, the order of excitation is used when designing absorber geometry. The reason for this is to match the natural frequency of the absorber to the exciting torque. This, like a linear vibration absorber, will theoretically counter the fluctuating torque and eliminate (or significantly reduce for the damped case) the vibration in the rotor. Equation 2.3 is used to find the natural frequency of the absorber.

2.2.1 Linearization

Assuming a small pendulum motion, ϕ, Equation 2.3 can be linearized to

$$m(\rho^2 + r^2)\ddot{\phi} + c_a\dot{\phi} + mrR\dot{\theta}^2\phi = -m(\rho^2 + r^2 + rR)\ddot{\theta} \tag{2.7}$$

This resembles the standard form for a forced vibration system,

$$\ddot{x} + 2\zeta\omega_n\dot{x} + \omega_n^2 x = f(t) \tag{2.8}$$

and the linearized natural frequency is easily calculated to be

$$\begin{aligned} \omega_n^2 &= \dot{\theta}^2 \frac{rR}{r^2 + \rho^2} \\ &\text{or} \\ \omega_n &= \dot{\theta}\sqrt{\frac{rR}{r^2 + \rho^2}} \end{aligned} \tag{2.9}$$

Equation 2.9 states that the natural frequency of the absorber varies linearly with the speed of the rotor, $\dot{\theta}$. This is one of the primary reasons CPVA's are so appealing. The absorber can be tuned to the order of excitation and will stay tuned at any rotor speed. Section 3.1 will discuss absorber tuning in more detail, and its affect on the system's response.

It is convenient to introduce the variable, $\tilde{n}$, to represent the tuning order of the absorber. Using Equation 2.9,

$$\tilde{n} \equiv \sqrt{\frac{rR}{r^2 + \rho^2}} \tag{2.10}$$

Equations 2.2 and 2.3 are non-linear, however, in practice it is often desirable to have the absorber operate in their linear range. The reason for this is discussed in the next section. Research has been done into cycloidal and epicycloidal paths, for the absorbers, such that the non-linearity is reduced or eliminated.

Equation 2.7 can also be used to determine an expression for the absorbers linear damping ratio, ζ_a, again by comparing it to a standard linear oscillator. Using Equation 2.9 this leads to the following relation:

$$\begin{aligned} 2\zeta_a \omega_n &= \frac{c_a}{m(\rho^2 + r^2)} \\ \zeta_a &= \frac{c_a}{m(\rho^2 + r^2)} \cdot \frac{1}{2}\frac{1}{\dot{\theta}}\sqrt{\frac{\rho^2 + r^2}{rR}} \end{aligned} \tag{2.11}$$

using the approximation $\dot{\theta} = \Omega$

$$\zeta_a = \frac{c_a}{2m\Omega\tilde{n}(\rho^2 + r^2)}$$

2.2.2 Non-Dimensionalization

It is desirable to be able to compare results from different systems that may have a variety of geometries, physical quantities and orders of excitation. To make this possible, non-dimensionalization of the equations of motion and parameters can be done. While previous researchers have also done this, for both circular and non-circular paths, it was only useful when comparing systems with equivalent tuning and excitation orders. A new method is developed here in which the excitation order is scaled out of the dimensionless equation of motion [9]. This method is outlined below.

Beginning with the full non-linear equations of motion given in Equations 2.2 and 2.3, previous methods have converted from time to rotor position, θ, as the independent variable. Since the rotor excitation, given by Equation 2.4, is dependent on the rotor position and the excitation order it is more convenient to define a new variable that will be used as the independent variable. Non-dimensional versions of the absorber position, and rotor speed are then defined and substituted into the original equations of motion using the chain rule. Next, a series expansion is used to simplify sines and cosines, and to reduce the complexity of the non-linear terms. A set of non-dimensional variables are defined for the damping, inertia and torque parameters, followed by the introduction of a "small" scaling parameter. Finally, after simplifications are made, the equations can be combined to uncouple the rotor motion from the absorber motion. The result is a non-dimensional first-order approximation, non-linear equation that contains absorber dynamics as a function of the applied torque.

To begin, several definitions must be made, and the chain rule applied. The definitions for the new independent variable, Ψ, the non-dimensional absorber path arc-length, s, and the non-dimensional rotor speed, ν, are given in Equation 2.12.

$$\Psi = n\theta, \quad s = \frac{r\phi}{\beta}, \quad \nu = \frac{\dot{\theta}}{\Omega} \tag{2.12}$$

β is a coefficient length scale to be defined later for convenience. Once the substitutions are made, the chain rule is used to change the independent variable from time into Ψ. The transformation uses the rules below:

$$\begin{aligned} \dot{(*)} &= \frac{d(*)}{dt} \\ (*)' &= \frac{d(*)}{d\Psi} \\ \frac{d(*)}{dt} = \frac{\partial\Psi}{\partial t}\frac{\partial(*)}{\partial\Psi} = n\dot{\theta}\frac{\partial(*)}{\partial\Psi} &= n\Omega\nu\frac{\partial(*)}{\partial\Psi} \\ \frac{d^2(*)}{dt^2} = (n\Omega)^2\nu\nu'\frac{\partial(*)}{\partial\Psi} &+ (n\nu\Omega)^2\frac{\partial^2(*)}{\partial\Psi^2} \end{aligned} \tag{2.13}$$

for example, using the chain rule:

$$\begin{aligned} \ddot{\theta} &= n\Omega^2\nu\nu' \\ \dot{\phi} &= \frac{\beta}{r}n\Omega\nu s' \\ \ddot{\phi} &= \frac{\beta}{r}(n\Omega)^2\left(\nu\nu's' + \nu^2 s''\right) \end{aligned} \tag{2.14}$$

Next, an expansion in s is used to eliminate sines and cosines, keeping only terms to order s^3. After making these substitutions and transformations, Equations 2.2 and

2.3 become

$$
\begin{aligned}
&\left(-\frac{mn^2\Omega^2R\left(s''\nu^2+\nu's'\nu\right))\,s^2}{2r^2}-\frac{mn^2\Omega^2R\nu^2s'^2s}{r^2}\right)\beta^3\\
&+\left(-\frac{2mn\Omega^2Rss'\nu^2}{r}-\frac{mn\Omega^2Rs^2\nu'\nu}{r}\right)\beta^2\\
&+\left(\frac{mn^2\Omega^2\left(r^2+Rr+\rho^2\right)\left(s''\nu^2+\nu's'\nu\right)}{r}\right)\beta\\
&+n\Omega^2\left(mr^2+2mRr+mR^2+m\rho^2+J\right)\nu\nu'=T_0+c_o\Omega\nu+T_\theta\sin(\Psi)
\end{aligned}
\tag{2.15}
$$

and

$$
\begin{aligned}
&-\frac{m\Omega^2R\nu^2s^3}{6r^2}\beta^3-\frac{mn\Omega^2R\nu\nu's^2}{2r}\beta^2+mn\Omega^2\left(r^2+Rr+\rho^2\right)\nu\nu'\\
&+\beta\left(mR\nu^2s)\Omega^2+\frac{mn^2\left(r^2+\rho^2\right)\left(s''\nu^2+\nu's'\nu\right)\Omega^2}{r}+\frac{c_an\nu s'\Omega}{r}\right)=0
\end{aligned}
\tag{2.16}
$$

Non-dimensional variables, Γ_0 and Γ_θ, for the applied torque and, μ_0 and μ_a, for the damping are then introduced, such that

$$
\begin{aligned}
\Gamma_0&=\frac{T_0}{J\Omega^2},\quad \mu_0=\frac{c_0}{J\Omega^2}\\
\Gamma_\theta&=\frac{T_\theta}{J\Omega^2},\quad \mu_a=\frac{c_a}{m\Omega(r^2+\rho^2)}
\end{aligned}
\tag{2.17}
$$

Substituting these definitions into Equations 2.15 and 2.16 yields:

$$
\begin{aligned}
&\left(-\frac{mn^2\Omega^2R\left(s''\nu^2+\nu's'\nu\right)s^2}{2r^2}-\frac{mn^2\Omega^2R\nu^2s'^2s}{r^2}\right)\beta^3\\
&+\left(-\frac{2mn\Omega^2Rss'\nu^2}{r}-\frac{mn\Omega^2Rs^2\nu'\nu}{r}\right)\beta^2\\
&+\frac{mn^2\Omega^2\left(r^2+Rr+\rho^2\right)\left(s''\nu^2+\nu's'\nu\right)}{r}\beta\\
&+n\Omega^2\left(mr^2+2mRr+mR^2+m\rho^2+J\right)\nu\nu'\\
&=J\Omega^2\big(\Gamma_0-\mu_0\nu+\Gamma_\theta\sin(\Psi)\big)
\end{aligned}
\tag{2.18}
$$

and

$$
\begin{aligned}
&-\frac{m\Omega^2 R\nu^2 s^3}{6r^2}\beta^3-\frac{mn\Omega^2 R\nu\nu' s^2}{2r}\beta^2+mn\Omega^2\left(r^2+Rr+\rho^2\right)\nu\nu' \\
&+\beta\left(mR\nu^2 s\Omega^2+\frac{m\mu_a n\left(r^2+\rho^2\right)\nu s'\Omega^2}{r}+\frac{mn^2\left(r^2+\rho^2\right)\left(s''\nu^2+\nu' s'\nu\right)\Omega^2}{r}\right) \\
&=0
\end{aligned}
\tag{2.19}
$$

The next step is to introduce a "small" parameter, ϵ, which is used for scaling. In this case, ϵ, like β, will be defined later for convenience. The purpose of using the specific exponents of ϵ below is to bring out the desired dynamic effects of interest at a given order in ϵ (see [1] for details). Several scaled dynamic variables and parameters are given by

$$
\begin{aligned}
s&=\epsilon^{\frac{1}{2}}z+\ldots, \qquad \nu=(1+\epsilon^{\frac{3}{2}}w)+\ldots \\
\Gamma_0&=\epsilon\tilde{\Gamma}_0, \qquad \Gamma_\theta=\epsilon^{\frac{3}{2}}\tilde{\Gamma}_\theta \\
\mu_0&=\epsilon\tilde{\mu}_0, \qquad \mu_a=\epsilon\tilde{\mu}_a
\end{aligned}
\tag{2.20}
$$

By making the above substitutions and expanding in ϵ, Equations 2.18 and 2.19 become:

$$
\begin{aligned}
&\left[J(\tilde{\mu}_0-\tilde{\Gamma}_0)\Omega^2\right]\epsilon \\
&+\left[\frac{\Omega^2\left(\beta\frac{J(r^2+\rho^2)}{(r^2+rR+\rho^2)}n^2 z''+Jrnw'-\tilde{\Gamma}_\theta Jr\sin(\Psi)\right)}{r}\right]\epsilon^{3/2}+O\left(\epsilon^2\right)=0
\end{aligned}
\tag{2.21}
$$

and

$$
\begin{aligned}
&\left[\frac{\beta\frac{J(r^2+\rho^2)}{(r^2+rR+\rho^2)^2}\Omega^2\left(\left(r^2+\rho^2\right)z''n^2+rRz\right)}{r}\right]\epsilon^{3/2} \\
&\left[+\frac{\frac{J(r^2+\rho^2)}{(r^2+rR+\rho^2)^2}\Omega^2\left(6nr\left(r\left(r^2+Rr+\rho^2\right)w'+\beta\tilde{\mu}_a\left(r^2+\rho^2\right)z'\right)-\beta^3 Rz^3\right)}{6r^2}\right]\epsilon^{5/2} \\
&+O\left(\epsilon^3\right) \\
&=0
\end{aligned}
\tag{2.22}
$$

Looking at the first order ϵ terms in Equation 2.21, the balance between the mean torque and the mean speed can be used, and Equation 2.6 is recovered. Setting the next highest order term, $(\epsilon^{3/2})$, to zero and solving for the non-dimensional rotor acceleration term, w', gives

$$w' = \frac{\tilde{\Gamma}_\theta}{n}\sin(\Psi) - \frac{\beta n}{r(1+\tilde{n}^2)}z'' \tag{2.23}$$

Substituting w' into Equation 2.22, effectively uncouples the the absorber dynamics from the rotor dynamics, leaving a single equation for the absorber dynamics that includes the forcing term from the applied torque.

It is convenient at this stage to define ϵ as a ratio of absorber to rotor inertia. In this way, the rotor/absorber coupling can be systematically taken to be small; as is the case in practical applications. This motivates a definition of ϵ as

$$\epsilon = \frac{m(r^2 + rR + \rho^2)^2}{J(r^2+\rho^2)} \tag{2.24}$$

which conveniently sets a coefficient to unity in the following development.

For simplification, β, and some other new parameters are defined. Many of the following parameters are defined this way such that the final equation is in a convenient form and similar to previous versions. β is defined by setting the coefficient of the ϵz^3 term to be equal to 1.

$$\beta = \sqrt{6n^2\frac{r}{R}(r^2+\rho^2)} \tag{2.25}$$

A new damping parameter, $\hat{\mu}_a$, is also defined to eliminate the use of n in the final equation.

$$\hat{\mu}_a = \frac{\tilde{\mu}_a}{n} \tag{2.26}$$

And finally, a torque amplitude parameter, Λ_θ, is defined as

$$\Lambda_\theta = \frac{\tilde{\Gamma}_\theta r(1+\tilde{n}^2)}{n^2\beta} \tag{2.27}$$

By making these substitutions the equation of motion can be simplified to the form shown in Equation 2.28.

$$z'' + \left(\frac{\tilde{n}}{n}\right)^2 z = \epsilon\left[-\hat{\mu}_a z' + z'' + z^3 - \Lambda_\theta \sin(\Psi)\right] \tag{2.28}$$

Since the purpose of this revised method is to eliminate the dependence on n in the final equation of motion, a parameter is needed to describe the tuning of the absorber relative to the excitation order. By replacing the explicit dependence on excitation order with a ratio of the tuning to excitation orders, the results are applicable to a much wider range of systems. This detuning parameter, σ, is defined as follows:

$$\tilde{n} = n(1+\epsilon\sigma) \tag{2.29}$$

Using the definition of σ given in 2.29, $(\frac{\tilde{n}}{n})^2$ becomes $1 + 2\epsilon\sigma + O(\epsilon^2)$ and $z'' = -z + O(\epsilon)$ which can be used in 2.28 to get the final form of the equation:

$$z'' + z = \epsilon\left[-\hat{\mu}_a z' - z - 2\sigma z + z^3 - \Lambda_\theta \sin(\Psi)\right] \tag{2.30}$$

Looking at the components of Equation 2.30, several comments can be made. The equation is made up of a linear ODE at order ϵ^0 with order ϵ corrections to account for various effects. First, the order ϵ^0 coefficient describes the linear absorber response. The order ϵ corrections includes the z^3 coefficient, which describes the non-linear effects of the absorber motion. Also of order ϵ is a z' component, representing the effects of damping on the solution. The z coefficient, which is derived from the z'' in Equation 2.28, accounts for the absorber/rotor interaction. Finally, the Λ_θ term, represents the fluctuating torque applied to the rotor, i.e. the forcing term of the system.

Equation 2.30 can be used to determine the scaled non-dimensional absorber motion, z, which can be used to calculate the scaled non-dimensional rotor acceleration, w', by using Equation 2.23. w' can then be used to calculate the dimensional form of the rotor acceleration, $\ddot{\theta}$ using the following relationships:

$$\ddot{\theta} = n\Omega^2 \epsilon^{3/2} \nu\nu'$$

and

$$\begin{aligned} \nu\nu' &= (1 + \epsilon^{3/2})\epsilon^{3/2} w' \\ &= \epsilon^{3/2} w' + O(\epsilon^2) \end{aligned} \tag{2.31}$$

which gives

$$\ddot{\theta} = n\Omega^2 (\epsilon^{3/2} w')$$

Method of Averaging

A useful way to describe the dynamics of the system is by approximating solutions of Equation 2.30 using the method of averaging. This results in equations for the amplitude and phase of the absorber motion. As previous researchers [1, 6, 7] have done, a polar coordinate transformation from z and z' to a and φ is introduced, such that

$$\begin{aligned} z &= a \sin(\Psi + \varphi) \\ z' &= a \cos(\Psi + \varphi) \end{aligned} \tag{2.32}$$

where a represents the slowly varying amplitude of the absorber motion in non-dimensional arc-length units, and φ is the phase angle between the applied torque and absorber motion. Using the method of averaging results in the following approximations:

$$a' = \epsilon \left[-\frac{\hat{\mu}_a}{2} a + \frac{\Lambda_\theta}{2} \sin(\varphi) \right] \tag{2.33}$$

$$a\varphi' = \epsilon \left[\left(\sigma + \frac{1}{2} \right) a - \frac{3}{8} a^3 + \frac{\Lambda_\theta}{2} \cos(\varphi) \right] \tag{2.34}$$

Using a method similar to previous researchers [5, 6], a relationship between the steady-state amplitude, $\bar{a}$, and the non-dimensional scaled torque parameter, Λ_θ, can be written, as in Equation 2.35. Under steady-state conditions, the slowly varying amplitude and phase (a and φ) are no longer varying, meaning $a' = \varphi' = 0$. Making this substitution, Equations 2.33 and 2.34 can be squared and added to obtain

$$\Lambda_\theta = 2\sqrt{\left(\frac{\hat{\mu}_a}{2}\bar{a}\right)^2 + \left(\frac{3}{8}\bar{a}^3 - \left(\sigma + \frac{1}{2}\right)\bar{a}\right)^2} \tag{2.35}$$

where $\bar{a}$ represents the steady-state value of a.

These results are useful because they reduce the equations to first order. Explicit solutions can be used to determine effects of various parameters on system response. Many of the figures in the next chapter are created using the above results.

CHAPTER 3

General Information

This chapter discusses some general information about CPVAs that are particularly useful for practical applications. Topics include absorber tuning, effects of mass and geometry on performance, and the influence of damping. Various figures are used to explain the effects of changing parameters, each created using equations derived in Chapter 2. Unless otherwise specified, all parameter values used to generate the figures in the chapter are given in Table 3. Chapter 4 discusses how these values are determined.

Parameter	**Value**
J	$0.063\ kg.m^2$
r	$0.039\ m$
R	$0.118\ m$
ρ	$0.0337\ m$
m	$0.52\ kg$
$\tilde{n}$	1.316
n	1.192
Ω	$10\pi rad/s$
c_a	$0.0004\ kg.m^2/s$

Table 3.1. System parameter values used in simulations

3.1 Tuning

When using pendulum absorbers in practice, there are general guidelines that are useful to know. One of the primary concerns should be the "tuning" of the pendulum absorbers. As discussed previously, many applications for pendulum absorbers operate at a specific order of excitation, n. A four-stroke internal combustion engine has a dominant excitation order equal to half the number of cylinders.

Tuning an absorber is done by adjusting its geometry such that its tuned order, $\tilde{n}$, given in Equation 2.10, is an appropriate percentage from the order of excitation. In practice, perfect tuning ($\tilde{n} = n$) is generally undesirable. The reason for this can best be explained by looking at the absorber response as the amplitude of fluctuating torque varies, see Figure 3.1.

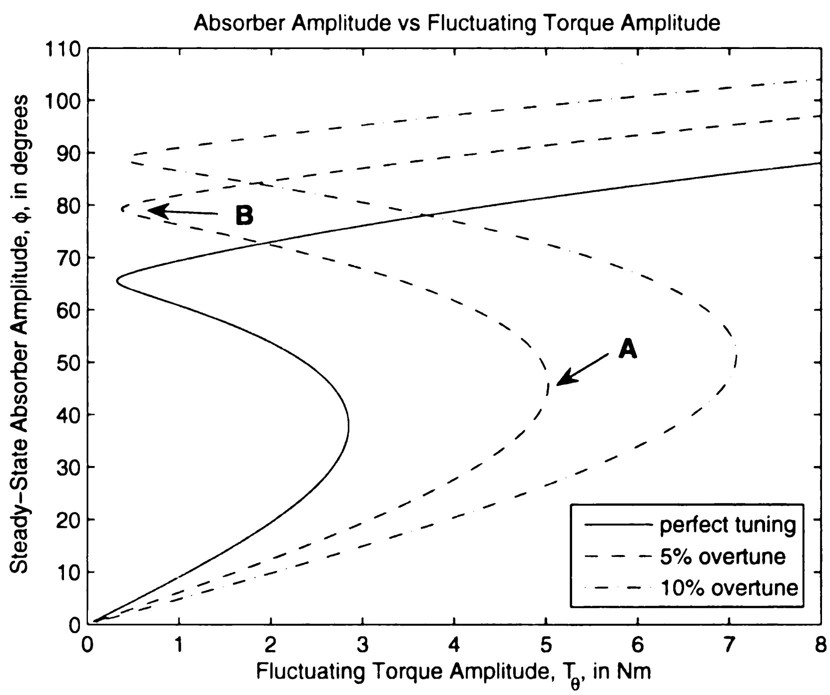

Figure 3.1. Absorber motion as a function of fluctuating torque amplitude for various levels of mistuning; created using Equation 2.35

Figure 3.1 contains a large amount of information. First, consider the curve corresponding to 5% overtuning. There are three distinct branches to this solution, the first branch is the positively-sloped line from the origin to the vertex marked A. In practice, this is the branch where operation is desirable. On this branch, the counter-torque generated by the absorber is out of phase with the applied torque, meaning it is absorbing vibration rather than amplifying it. According to the stability study done by Alsuwaiyan [1], this lower branch is a stable solution for a single absorber, or absorbers acting in unison up to a certain torque level. However, the next branch is unstable. This would be the middle, negatively-sloped curve between points A and B. The final, topmost branch, is also stable, but undesirable. When the absorber operates on this branch, not only is it associated with very large absorber angles, it also creates a torque in phase with the applied torque, causing an increase in the rotor's fluctuation, which in many cases can be dangerous.

The absorber motion follows a hysteretic behavior between the upper and lower branches. On the lower branch, as the fluctuating torque is increased, the absorber's magnitude will continue to increase, almost linearly, until operating near point A. At (or near, since these calculations are based on approximations) this point the absorber motion goes through a "jump" to the upper branch and causes an increase in the torsional vibrations. Once operating on this upper branch, the fluctuating torque must be reduced to (or near) point B before the motion will again experience this "jump" behavior back down to the lower branch.

To help stay on the lower branch where the absorbers are acting as intended, the absorbers should be tuned for their specific application. When the system is tuned exactly to the order of excitation ($\tilde{n} = n$), the range of fluctuating torque that they are capable of counter-acting is extremely limited. However, as will be shown subsequently, while in this region, they do a much better job of absorbing the torsional vibration. As tuning is increased further from perfect tuning, the "safe" range of operation increases. This is shown by the 5% and 10% overtuned cases ($\tilde{n} = 1.05 \cdot n$ and $1.10 \cdot n$). However, increasing the amount of detuning is not always desirable, as is described in the following.

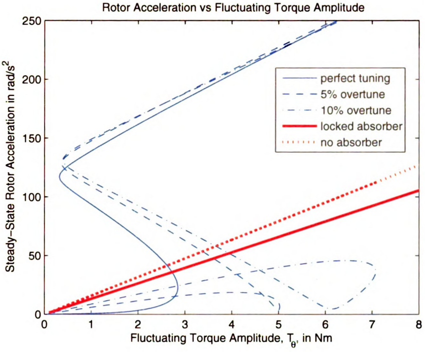

Figure 3.2. Rotor acceleration as a function of absorber tuning; created from Equations 2.35 and 2.31

The purpose of adding absorbers is to reduce torsional vibration in the rotor, which can be measured using the magnitude of the rotor's acceleration, see Figure 3.2. As a comparison, there are two straight lines plotted on Figure 3.2 that represent the rotor acceleration with the absorber locked at its vertex and with the absorber completely removed. Adding the absorber, but having it locked does reduce the vibration slightly, but this is only due to the flywheel effect, i.e. the additional mass of the absorber adds inertia to the system. By allowing the absorber to swing, it generates a counter-torque on the rotor, which reduces the effect of the applied fluctuating torque. As mentioned before, having a perfectly tuned absorber results in the best vibration reduction (lowest acceleration), but only over a very limited range of applied torque amplitudes. By detuning the absorber, the useful range is increased, but with a slight sacrifice in performance.

When tuning an absorber, it is necessary to find the balance between performance and a range of operation that will avoid unwanted jumps to the amplifying branch of the solution. Alsuwaiyan [1] calculated a formula for predicting the amplitude at which absorbers will "jump". He also calculated when a multi-absorber system will lose its syncronous motion. Section 2.1 briefly discussed multiple absorber systems, and that single absorber systems can be used to model multiple absorbers when they are behaving in unison.

3.2 Mass

There are ways of improving absorber performance without changing the tuning, which could result in unwanted behavior. One way is to increase the mass of the absorbers. From Equation 2.5, the counter-torque generated by the absorber is proportional to the mass of the absorber. Increasing absorber mass increases the inertia of the absorbers, which increases their influence over the rotor, without having to increase their swing angle. Effectively, this delays the onset of the jump to the (undesirable) upper-branch solution, see Figures 3.2 and 3.1. Absorbers with greater inertia are less excited by the vibration of the rotor, which means that for the same conditions, absorbers with greater mass will have smaller swing angles. The drawback to increasing the mass is similar to the flywheel effect, system response becomes slower, possibly sluggish. This is often not acceptable. Figure 3.3 shows several examples of the difference in vibration reduction between a 1 kg absorber and a 1.5 kg absorber.

3.3 Radius, R

Another way to improve absorber performance is to increase the distance of the absorber from the center of rotation, or R from Figure 2.1. The dominant term (for small absorber angles) in Equation 2.5 is mR^2, meaning the torque created by the pendulum absorber is proportional to R^2. It can be shown that the reduction in rotor vibration is increased proportionally with R^2. This allows smaller absorbers to have greater leverage on the rotor. Again, for the same conditions, the absorbers will not only swing less, but generate a larger amplitude counter-torque, improving vibration reduction. As with the increase in mass, the benefits from increasing R also become drawbacks when the absorber motion generates a counter-torque in phase with the applied torque. In this case, the the effect of vibration amplification is also increased.

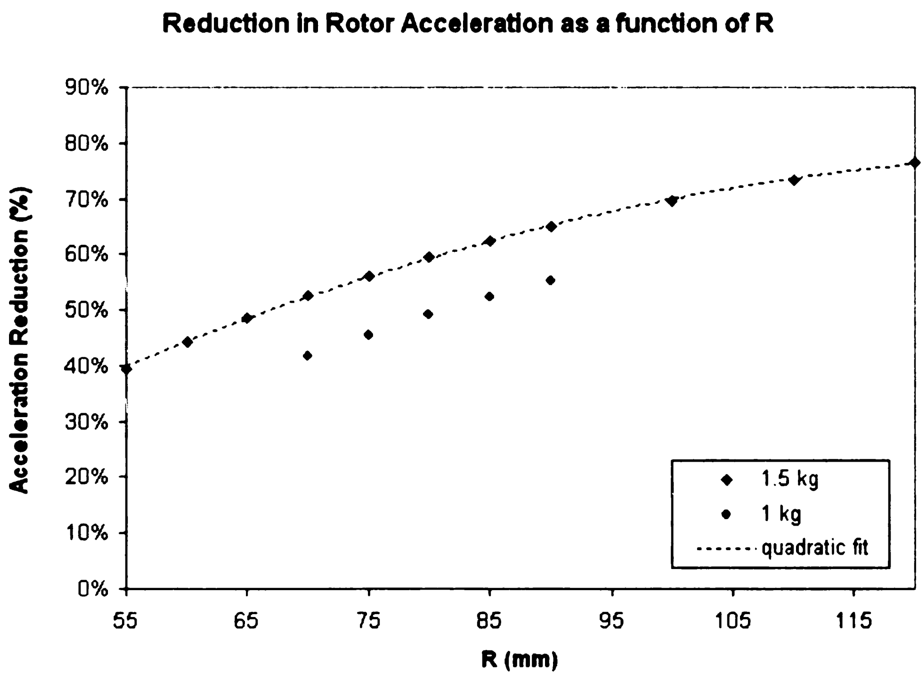

Figure 3.3. Vibration reduction as a function of radius, R

Several simulations were run using numerical integration of Equations 2.2 and 2.3 to show how the radius influenced vibration reduction. The results are shown in Figure 3.3. The figure shows how increasing the radius from 70 mm to 90 mm had an improvement similar to increasing the mass by 50%.

In general, increasing the distance between the center of rotation and the absorber's center of gravity will improve performance. This means that increasing r will also give the absorber greater leverage without having to increase the swing angle.

3.4 Damping

The absorber damping plays a similar role to the damping in a frequency tuned absorber system. Theoretically, a system without damping has the ability to eliminate vibration in the primary system completely. However, the resonant response, where the absorber is amplifying instead of absorbing vibration can have infinite amplitude. Increasing energy dissipation in the system reduces both these effects, having the drawback that absorber performance is also reduced.

Damping, however, is not entirely undesirable. Absorber damping also has a similar influence as overtuning, described in Section 3.1. Figures 3.4 and 3.5 show how absorber damping can increase the usable range for the absorber operation. Damping can also be a significant factor in transient behavior, as discussed in the next chapter.

Similar to the plots used to describe the benefits of tuning, plotting various levels of damping demonstrate the advantages and disadvantages the absorber damping has on the absorber performance. Focussing on absorber motion, Figure 3.4 shows how increased damping can extend the absorber's usable range. A huge advantage possible with increased damping is that the hysteretic behavior of the absorber motion is

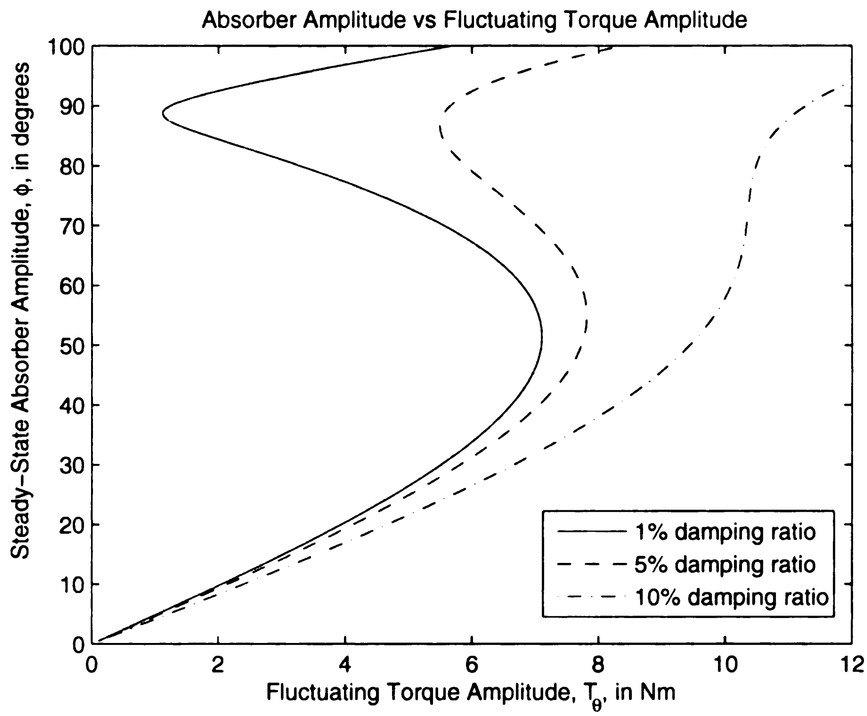

Figure 3.4. Absorber damping influence on absorber motion; created using Equation 2.35, damping ratio defined in Equation 2.11

significantly improved. With less damping, a system may suffer catastrophic failure if a jump to amplifying behavior occurs, where a system with more damping can be brought back under control by a slight reduction in the fluctuating torque. In terms of an automotive application, it could mean the difference between shutting off the engine completely or simply closing the throttle slightly. As Figure 3.5 shows, increased damping does have a small influence over the ability of the absorber to reduce vibration, but not nearly as dramatic as the effect of overtuning.

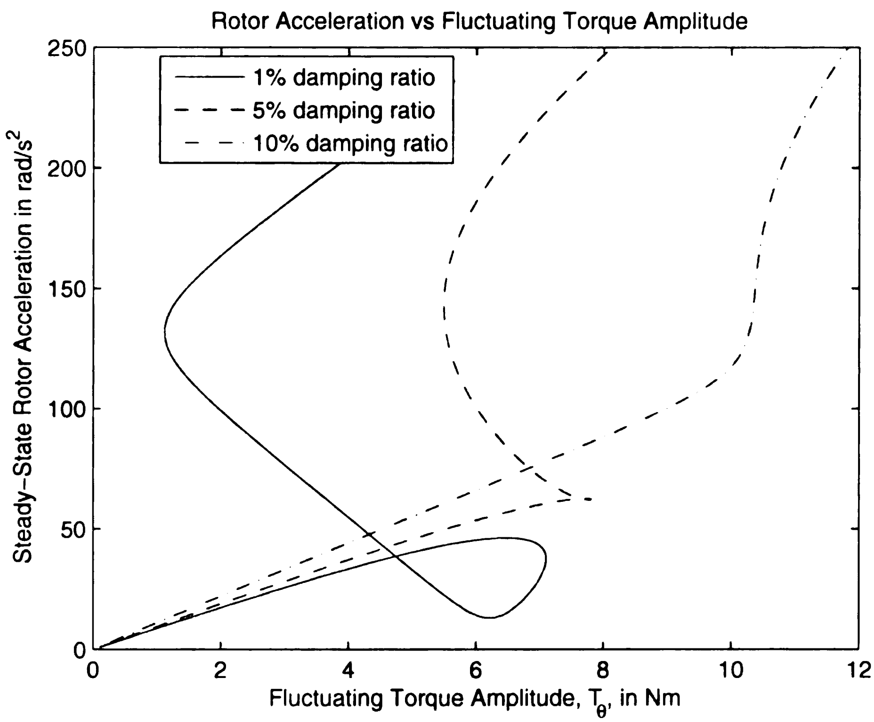

Figure 3.5. Absorber damping influence on rotor acceleration; created using Equation 2.35, damping ratio defined in Equation 2.11

CHAPTER 4

Experimental Work

This chapter outlines the experimental apparatus and tests that were run. Before any transient response testing can be done, certain parameter values had to be determined in order to compare results to theoretical predictions. Once the system parameters are known, various input variables, such as fluctuating torque amplitudes and the order of excitation, are changed while the system is running.

4.1 Experimental Setup

A more detailed description of the experimental apparatus is given in [8]. An overview of the device is presented here. Past researchers have also used this particular apparatus for pendulum absorber testing. Not only is this device the only known (as of the writing of this thesis) test rig capable of measuring the response of the absorbers it can also accomodate various parameter changes. It has the ability to generate fluctuating torque over a broad range of amplitudes and excitation orders, as well as the space for various types of absorbers. Up to four absorbers can be accommodated.

Figure 4.1 shows the actual test rig. The unit consists of a shaft, mounted vertically in an aluminum frame. An electric motor (B) attached to the top end, spins the shaft on two bearings (C). Near the lower end, between the bearings, is a ro-

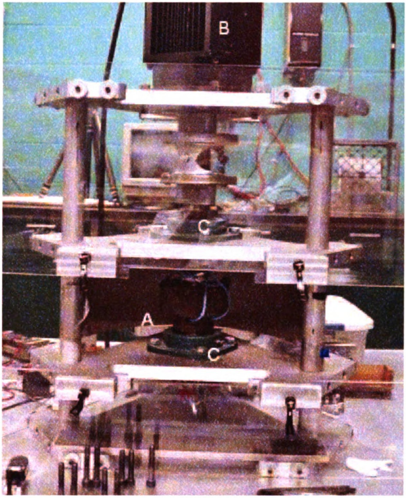

Figure 4.1. Experimental apparatus: (A) Rotor, (B) Motor, (C) Bearings

tor/flywheel (A), machined to accept up to four absorbers or other attachments. The absorbers used in this work are shown in Figure 4.2. Under the lower bearing, cables pass through a slip ring into differential encoders mounted on the rotor/absorbers that measure the position of the absorbers. The encoder, absorber and its base are shown in Figures 4.2 and 4.3. There is also an encoder on the motor that emits 1000 pulses per revolution. This is used to record the instantaneous position and speed of the rotor.

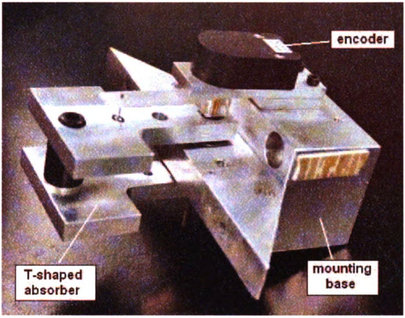

Figure 4.2. Circular path, T-shaped absorber assembly in "free" configuration

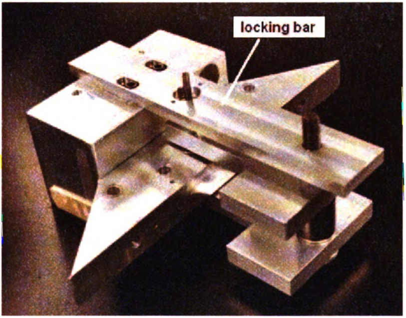

Figure 4.3. Circular path, T-shaped absorber assembly in "locked" configuration

Feedback controls are used to control the motor. Two computers are used, one for the mean component of the torque (to control mean speed), and another generates a sine wave signal (the fluctuating component of the torque). The speed of the rotor is fed into a computer that slowly increases or decreases the output voltage to maintain the set speed. Unfortunately, supplying a constant voltage to the motor torque controller does not produce an absolutely constant mean speed. Left unchecked, the mean speed slowly drifts from its originally set value. This is easily corrected by this computer, which is used to monitor the mean speed of the rotor and adjust the voltage supplied to the motor to keep the mean rotor speed at the set level. The result is a very slow variation in the mean speed about the set value. For more precise testing, this problem should be corrected, but for the purposes of this work, the variation does not cause any major problems.

The angular position of the rotor is fed into the second computer where it is used as a time base to generate the voltage signal for the fluctuating torque. This can be altered on-the-fly to any desired order, n. The voltages from the two computers are added together before being sent into the motor controller where the voltage signal is used to control the applied torque. A third computer is used to log data including applied torque, instantaneous rotor speed and absorber positions. A schematic of the experimental setup is shown in Figure 4.4.

Note

For the experimental tests given in this chapter, the test apparatus is fitted with two (2) equally sized absorbers. Absorber amplitude results are presented as the average amplitude of the two absorbers. All test results presented here have syncronous absorber motion. Many of the results presented in this chapter include rotor acceleration, which is not directly measured experimentally. The acceleration is calculated by numerically differentiating the instantaneous rotor speed, which is directly measured.

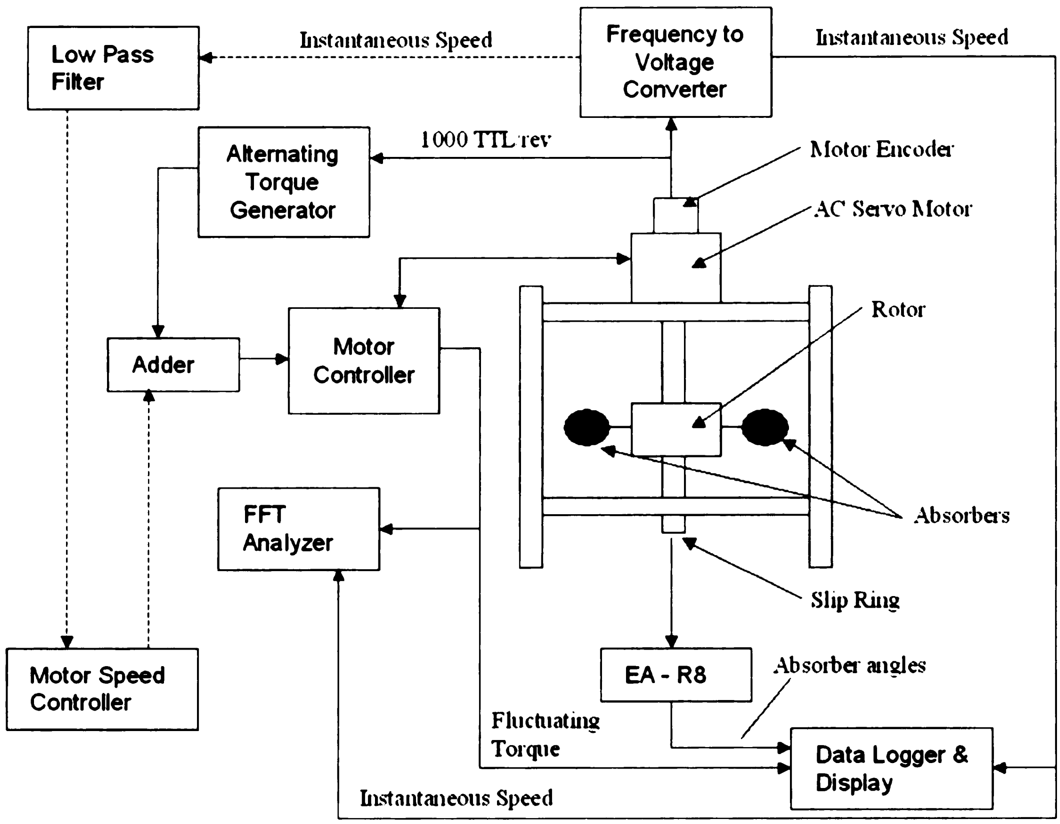

Figure 4.4. Schematic of experimental setup (from [8])

4.2 System Parameter Values

Before any experimental results can be analyzed and compared to theory, certain parameters must be determined from the test apparatus. These fall into two classes: the first are directly measurable, i.e. mass, radius, etc. The second have to obtained experimentally and include the rotational inertia of the rotor, and the amount of damping in the absorbers. It is also interesting to know the damping in the rotor. However, the current test apparatus has such a small amount of friction in the rotor that the torque required (mean torque) to spin the rotor is so small that it is difficult to measure. Since the rotor's damping has little to do with the steady-state dynamics of the system, other than the mean speed of the rotor, testing to determine it was not done, although it can be estimated from the ratio T_0/Ω.

The inertia of the rotor was found by using the simple principle that the fluctuating torque applied to a rigid rotor is proportional to its rotational acceleration. The constant of proportionality, J, is the rotor's rotational inertia.

$$T_\theta = J\|\ddot{\theta}\| \tag{4.1}$$

To calculate the inertia, a torque with a constant fluctuating amplitude (of the form given in Equation 2.4) is applied to the rotor and its motion is recorded to be used with Equation 4.1. This was done using two different fluctuating torque amplitudes. The inertia of the system without the absorbers present is found to be approximately 0.063 to 0.067 $kg.m^2$.

To find the absorber's damping, a log decrement method was used. With a single absorber free to swing and the other absorber locked, the system is run with a constant fluctuating torque applied until it reached a steady state, then the fluctuation torque was suddenly stopped and the decay in the free absorber's swing was recorded. Using Equations 4.2, the damping ratio for each absorber can be calculated. As with the rotor inertia, the tests were performed twice for each of the two absorbers, using different torque amplitudes.

$$\frac{\zeta_a}{\sqrt{1-\zeta_a^2}} = \frac{ln(\frac{a_0}{a_n})}{2\pi.x_n} \tag{4.2}$$

where a_0 and a_n are the amplitudes at the first and nth peak of the absorber's decay. x_n is the integer number of peaks used in the calculation. The results are given in Table 4.2. It should be noted that the damping ratio is expected to be a function of the mean rotor speed, Ω, as shown in Figure 2.11. The values given below were obtained at a mean speed of 10π rad/s.

Absorber	Damping Ratio, ζ_a
1	0.0042, 0.0043
2	0.0030, 0.0036

Table 4.1. Damping ratios for absorbers

Measurable parameter values, used in the simulations in this chapter, are given in Table 4.2. Parameters marked with an * are estimated from other measured quantities.

Parameter	Value
r	0.039 m
R	0.118 m
ρ	0.0337 m
m	0.26 kg each 0.52 kg total
T_0*	0.25 $N.m$
c_0*	0.0004 $kg.m^2/s$

Table 4.2. Measurable system parameter values used in simulations

A small amount of research was done to investigate certain parameter values for actual automotive applications, namely, the powertrain rotational inertia and damping. It has been a topic of discussion as to how much of the powertrain should be included when calculating rotational inertia. For a vehicle equipped with an automatic transmission, components downstream of a torque converter may be less significant than others. Certainly, the crankshaft, connecting rods and pistons in the engine should be included in a calculation of this type. While sizes of engines will vary, a common range of realistic rotational inertias for an average-sized engine is 0.05 $kg.m^2$ to 0.15 $kg.m^2$.

Friction in an internal combustion engine is also a function of many different variables including size, type of motor oil, configuration, etc., and it is likely to not be entirely viscous as modeled in this work. As an approximation, a viscous damping coefficient for an average-sized internal combustion engine is likely to fall in the range of 0.05 $\frac{kg.m^2}{s}$ to 0.2 $\frac{kg.m^2}{s}$.

4.3 Transient Tests

Two basic tests are performed to investigate the behavior of the absorbers during changes in the system. The tests consist of step changes in the order of excitation and the fluctuating torque amplitude. In each case, the system is allowed to reach a steady state before the step change is implemented.

When changing excitation order, specific values of 1.192 and 2.384 are chosen. These values are used to attempt to model a situation that might be seen in practice. As mentioned in the introduction, vehicles equipped with cylinder deactivation technology are excellent candidates for pendulum absorbers. To use absorbers in practice, a certain amount of overtuning is desirable to avoid jumps to amplifying solutions. Since the test rig has a fixed tuning order of $\tilde{n} \approx 1.316$, $n = 1.192$ makes the system roughly 10.4% overtuned. When the vehicle is in its normal mode, the excitation order would be twice the value as when it is in reduced-cylinder mode. Meaning that $n = 1.192$ will represent operation in reduced-cylinder mode and $n = 2.384$ represents operation in normal mode.

4.3.1 Simulations

Many of the experimental results in the following section are accompanied by simulation results. Simulations refer to a numerical solution to Equations 2.2 and 2.3. For each simulation, the parameters used are those determined from the experimental apparatus, with the exception of the mean torque and rotor damping. Because these values are difficult to determine, they are fixed to give the appropriate measured mean speed.

4.3.2 Excitation Order Step Change

High Frequency to Low Frequency: Locked Absorbers

To establish a baseline, a test is run with the absorbers locked. In this configuration, the system should behave as a single rotating inertia and have an equation of motion given by Equation 4.3, where I_{zz} is the combined inertia of the rotor and locked absorbers.

$$T(t) = I_{zz}\ddot{\theta} + c_0\dot{\theta} \tag{4.3}$$

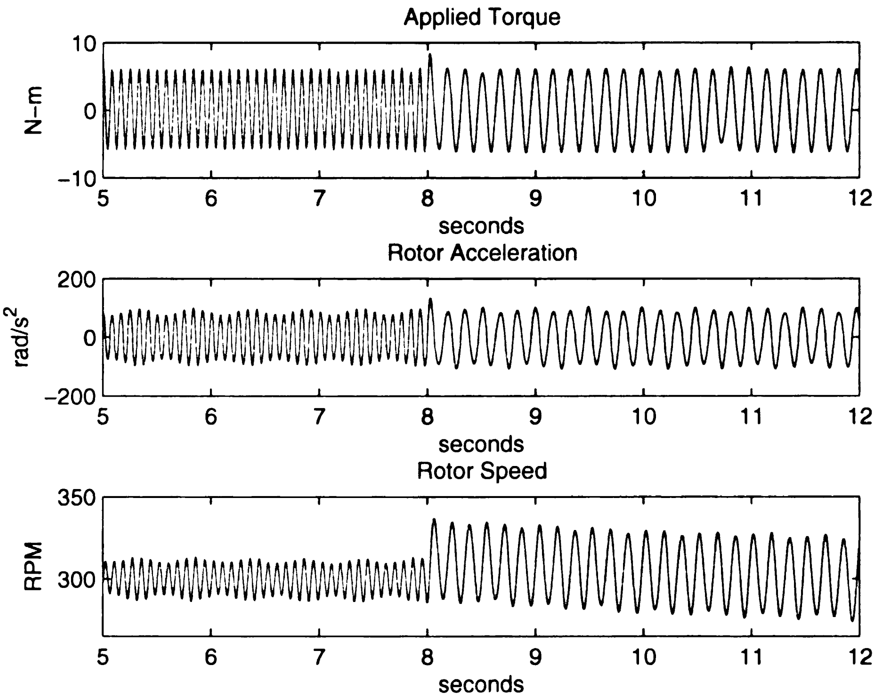

Figure 4.5. Experimental Results: order step change from n = 2.384 to n = 1.192 at $T_\theta = 6.2N.m$, locked absorbers

Figure 4.5 shows the acceleration, $\ddot{\theta}$, and speed, $\dot{\theta}$, of the rotor during a step change in the excitation order, n. This is what might be seen in an engine when switching to reduced-cylinder mode. While it is not transient behavior, it should be noted here that the steady-state amplitude of the acceleration is the same for both excitation orders, but the steady amplitude of the speed is doubled for half the excitation order. This is expected, and can be explained by using Equation 4.4.

$$\begin{aligned}
\theta_{ss} &= \Omega t + \theta_0 \sin(n\Omega t) \\
\dot{\theta}_{ss} &= \Omega + \theta_0 n\Omega \cos(n\Omega t) \\
\ddot{\theta}_{ss} &= -\theta_0 (n\Omega)^2 \sin(n\Omega t)
\end{aligned} \tag{4.4}$$

It can be assumed that the steady-state rotor motion can be approximated as in Equation 4.4 when a torque given by Equation 2.4 is applied. There is a constant increasing term as the rotor spins at some mean speed, Ω, along with a small perturbation in that motion with amplitude θ_0. It can also be assumed that amplitude of the rotor acceleration is dependent on the fluctuating torque, as in Equation 4.3. Algebraically, if the fluctuating torque amplitude is constant and the excitation order is halved, the steady-state magnitudes of the acceleration and speed are constant and doubled, respectively.

Another point to notice is the rotor's speed transition. Due to the conditions of the step change (the order is set to decrease when the torque is at a positively sloped zero-crossing), the applied torque is positive for a slightly longer period of time. This causes the mean speed of the rotor to temporarily increase. This is shown in Figure 4.6 in both the experimental data and simulation. If the step change occurred when the torque is decreasing, the opposite is true. The mean speed would temporarily decrease. The transition back to the steady mean speed (300 RPM) is approximately the same in both instances and is dictated by the homogeneous solution of equation 4.3, which is a first order ODE in the rotor speed, $\dot{\theta}$. It is easy to show that the

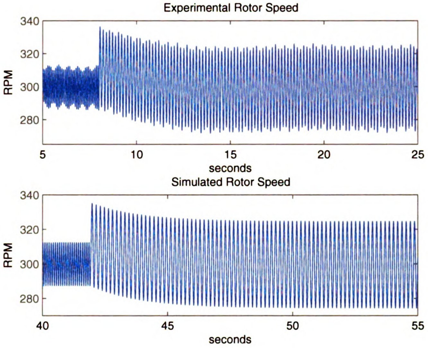

Figure 4.6. Experimental and Simulated Results: rotor speed during order step change from $n = 2.384$ to $n = 1.192$, $T_\theta = 6.2N.m$, locked absorbers

associated time constant, τ, is

$$\tau = -\frac{I_{zz}}{c} \tag{4.5}$$

This dictates the rate for the transient motion to decay.

High Frequency to Low Frequency: Free Absorbers

The previous test is now repeated with the absorbers free. This time, the torque level is slightly lower (5.25 Nm) to keep the absorbers from swinging too far, possibly causing damage. At $n = 2.384$, the excitation is far enough away from the tuning of the absorbers that they are not significantly excited. However, when the excitation order is halved, the absorbers are now only 10% away from perfect tuning, which means the absorber amplitude should be much larger. Figure 4.7 shows the experimental and simulated absorber motion during the step change.

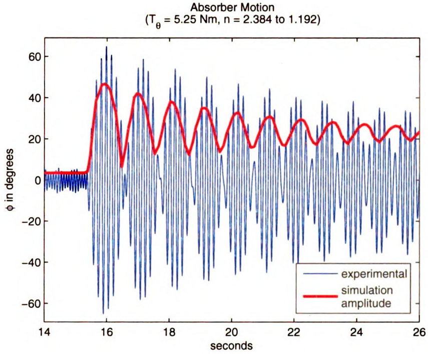

Figure 4.7. Experimental and Simulated Results: absorber motion during order step change from $n = 2.384$ to $n = 1.192$, $T_\theta = 5.25N.m$

The general trend of the absorber amplitude shown in Figure 4.7 is the same in both experimental and simulated results; an initial overshoot followed by settling to a new larger steady-state amplitude. The results from the method of averaging (Equations 2.33 and 2.34) were also used to predict transient behavior, but because this torque level is close to the jump point, the method of averaging simulation resulted in a jump in the absorber's motion. This is likely a consequence of the step change initial conditions not lying close enough to the appropriate basic of attraction. Those results are not included here, however, similar results are presented in a later section of this chapter.

The beating that occurs after the step change is expected. Typically, a beating response comes from two frequencies that are close to one another, which is the case in this system. At steady state, the transient (free) vibrations have decayed away, so the response is dominated by the forcing frequency, n, in this case. Immediately after the step occurs, the system once again has both a free and forced response until the free response component decays. The corresponding frequencies are $\tilde{n}$ and n, which are only different by approximately 10%.

Although the general trend between the simulation and the experiment are correct, the amplitude and the resulting frequencies are slightly off. This discrepancy is likely due to the variation in the experimental rotor's mean speed, which determines the excitation frequency and as a result, the response frequency. As the rotor spins with

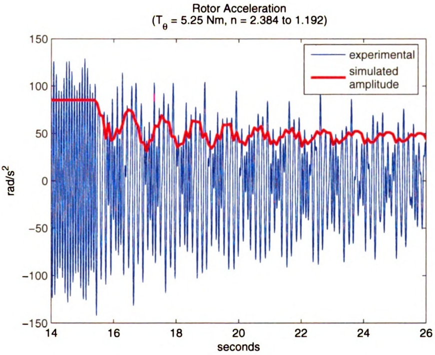

Figure 4.8. Experimental and Simulated Results: rotor acceleration during order step change from $n = 2.384$ to $n = 1.192$, $T_\theta = 5.25N.m$

a slightly different mean speed, the two results slowly drift out of phase with each other. A possible source for the amplitude difference is likely to be the form of the damping. It may be much more complicated than simple viscous damping, which would certainly influence the amplitude of the response.

The absorber amplitude is also extremely dependent on the absorber tuning. The variation in the rotor's mean speed changes the frequency at which the excitation occurs. This change translates into a slight change in tuning, which can dramatically affect response amplitude, as shown in Figures 3.1 and 3.2.

Figure 4.8 demonstrates that when the excitation order is suddenly halved to be close to $\tilde{n}$, that the torsional vibration is reduced. Although the reduction in $\ddot{\theta}$ is only about 40% it should be noted that there is a considerably large amount (%) of overtuning in the system ($\tilde{n} \approx n + 10\%n$).

Low Frequency to High Frequency: Free Absorbers

Figure 4.9 shows how the absorbers behave as the excitation order is changed from a lower order (1.192) to a higher order (2.384). As expected, the absorber steady-state amplitude is much smaller when excited by the 2.384 order torque because of the dramatic amount of mistuning ($\tilde{n}$ is nearly 50% below n, or undertuned). A smaller torque value is used in this experiment again to avoid large absorber amplitude responses at the lower excitation order.

Figure 4.10 shows the associated vibration (or acceleration) that results in the rotor due to the increase in the excitation order. Again, the initial overshoot is followed by a beating exponential decay to the new higher steady-state value. As mentioned in Chapter 1, in practice, the high level of vibration seen at $n = 2.384$, which corresponds to an engine operating with all cylinders, is controlled by other means. Automotive engines are typically very well balanced in this configuration.

Experimental and simulation differences in the amplitude and phase can be ex-

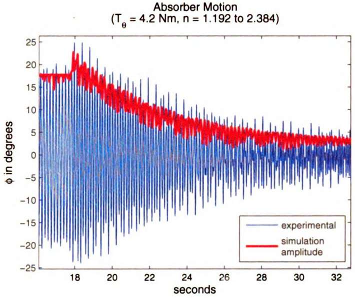

Figure 4.9. Experimental and Simulated Results: absorber motion during order step change from $n = 1.192$ to $n = 2.384$, $T_\theta = 4.2N.m$

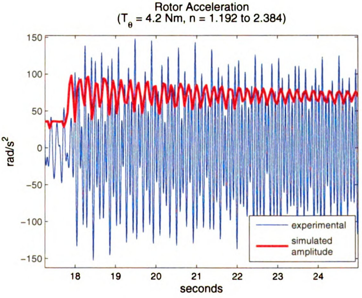

Figure 4.10. Experimental and Simulated Results: rotor acceleration during order step change from $n = 1.192$ to $n = 2.384$, $T_\theta = 4.2N.m$

plained using the same arguments as the step change from a high to a low excitation order. The general trend, however, is very close between simulation and experimental results.

4.3.3 Fluctuating Torque Amplitude Step Change

Increase in Fluctuating Torque: Locked Absorbers

As in the previous section, the first test is run with the absorbers locked. In this case, the behavior is again exactly as expected. An increase in the amplitude of the fluctuating torque increases the amplitude of the acceleration, which results in an increase in the fluctuation in the speed, this time due to the θ_0 term in Equation 4.4 since n and Ω are constant. Figure 4.11 shows how the rotor responds during a step change in the fluctuating torque amplitude.

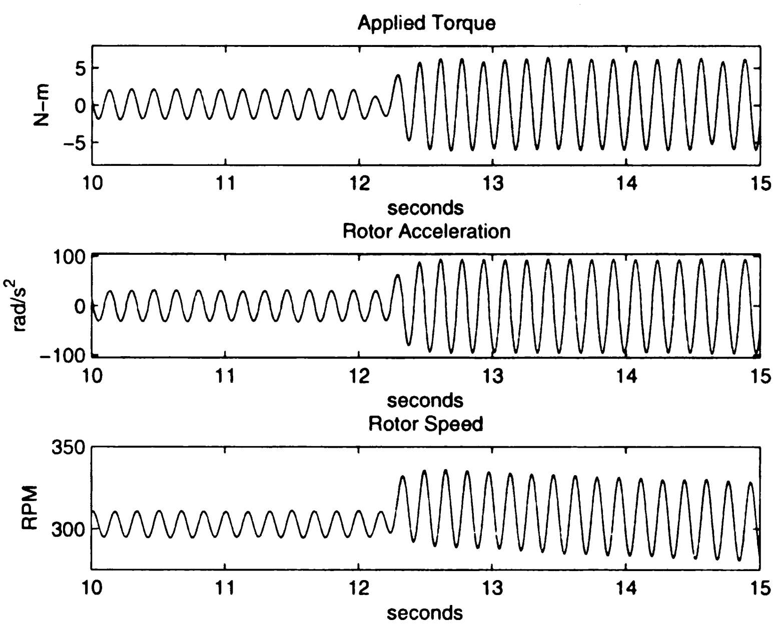

Figure 4.11. Experimental Results: step change in fluctuating torque amplitude from $T_\theta = 2Nm$ to $T_\theta = 6.2Nm$, $n = 2.384$, locked absorbers

Again, looking at the disturbance in the mean rotor speed shows that it is slightly increased due to the increase in fluctuating torque. The step occurs while the torque is increasing, which accelerates the rotor, increasing the mean speed. The decay in this transient behavior is exponential. Figure 4.12 gives a closer look at the experimental and simulated rotor speed. As is mathematically predicted, the steady-state amplitude of the fluctuation in speed varies linearly with the fluctuating torque amplitude.

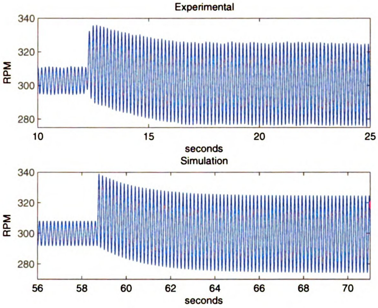

Figure 4.12. Experimental and Simulated Results: rotor speed during step change in fluctuating torque amplitude from $T_\theta = 2Nm$ to $T_\theta = 6.2Nm$, $n = 1.192$, locked absorbers

Increase in Fluctuating Torque: Free Absorbers

For the following tests, not only are experimental and simulated results presented, but results from numerical integration of the averaged equations, Equations 2.33 and 2.34, are used to predict transient behavior. While the method of averaging is only valid for slowly varying amplitudes and phases, all three results are in close agreement. It should be noted that this slowly varying requirement can be relaxed if the step changes are considered to be only an expression of a change in the intitial conditions. This is explained further at the end of this chapter, see Figures 4.17 and 4.18.

Figure 4.13 shows the behavior of the absorber when the fluctuating torque amplitude is increased from 2 $N.m$ to 4.2 $N.m$. Both the simulation and the averaged amplitudes match closely with the experimental results. Discrepancies in amplitude and frequency can be explained as previously. All three results show an amplitude overshoot followed by the beating behavior. As expected, the steady-state amplitude after the step change is larger than before.

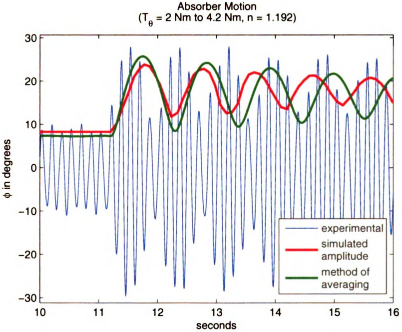

Figure 4.13. Experimental and Simulated Results: absorber motion during fluctuating torque amplitude step change from $T_\theta = 2N.m$ to $T_\theta = 4.2N.m$, $n = 1.192$

Figure 4.14 demonstrates how the rotor behaves during the step change in fluctuating torque. In this case, Equation 2.23 is used with Equations 2.33 and 2.34

to calculate the amplitude of the rotor acceleration. The same general trends are observed.

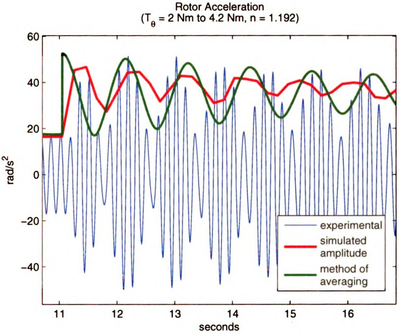

Figure 4.14. Experimental and Simulated Results: rotor acceleration during fluctuating torque amplitude step change from $T_\theta = 2Nm$ to $T_\theta = 4.2Nm$, $n = 1.192$

Decrease in Fluctuating Torque: Free Absorbers

Figures 4.15 and 4.16 give the results of the step change from a higher fluctuating torque amplitude to a lower fluctuating torque amplitude. Similar comments can be made about the agreement between experimental, simulated and averaged approximation results. The behavior of the absorber and rotor acceleration follows the same type of pattern as before. The decay of transient motion to the new steady amplitude is exponential, and it has the same beating behavior seen in many of the previous tests.

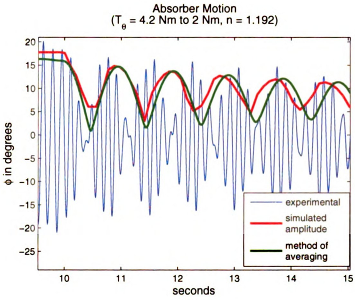

Figure 4.15. Experimental and Simulated Results: absorber motion during fluctuating torque amplitude step change from $T_\theta = 4.2Nm$ to $T_\theta = 2Nm$, $n = 1.192$

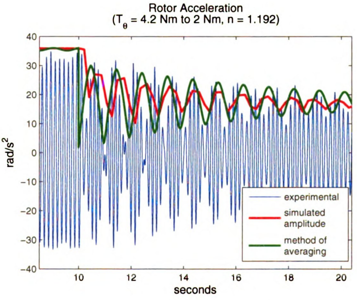

Figure 4.16. Experimental and Simulated Results: rotor acceleration during fluctuating torque amplitude step change from $T_\theta = 4.2Nm$ to $T_\theta = 2Nm$, $n = 1.192$

Discussion

These results appear similar to the results obtained when the excitation order was changed from low frequency to high frequency. The resulting amplitude may look similar, but the actual behavior of the absorber relative to the rest of the system is very different. This may be better explained using Figures 4.17 and 4.18, which show simulated phase portraits for two cases of an excitation order change and a fluctuating torque amplitude change. They are obtained by numerical integration of the averaged equations 2.33 and 2.34. In both cases, the final state is the same.

Before the change in excitation order, indicated as the initial state in Figure 4.17, the absorber is only excited to a relatively small amplitude. This is because the absorber is so far out of tune from the excitation order. Notice also, that the absorber motion is in phase with the applied torque, i.e. it is amplifying the vibration in the rotor. Once the order is changed, the absorber is tuned much closer to the excitation, which results in an increase in amplitude. The torque level remains constant, but now the excitation is more in tune with the absorber. After the change, the absorber motion is 180° out of phase with the applied torque, so the counter-torque is opposite the applied torque, and a vibration reduction in the rotor occurs.

Considering a similar situation, but now the excitation order remains constant as the torque level is increased. The results from the numerical intergration of the averaged equations are shown in Figure 4.18. Again, the amplitude of the absorber is only excited to a relatively small amplitude until the step change. Then the amplitude increases to the same steady value as in Figure 4.17. This time, however, both the initial state and the final state are 180° out of phase (absorbing rather than amplifying vibration). Since, the tuning has not changed, the increase in amplitude comes from being excited by a larger torque amplitude. While the two cases appear similar, there are significant differences between a step change in excitation order and a step change in fluctuating torque amplitude.

The use of the averaged equations here indicates a possible way to efficiently find the bounds on the overshoots, beating frequency and the decay rates. This is left for future work.

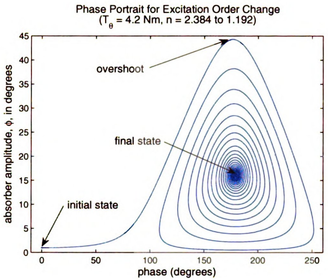

Figure 4.17. Simulated Results: phase portrait for excitation order change from $n = 2.384$ to $n = 1.192$, $T_\theta = 4.2N.m$

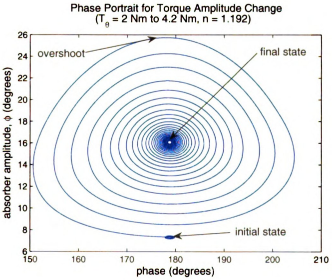

Figure 4.18. Simulated Results: phase portrait for fluctuating torque amplitude change from $T_\theta = 2N.m$ to $T_\theta = 4.2N.m$, $n = 1.192$

CHAPTER 5

Conclusions

Over the past years many researchers have worked on various aspects of the design and performance of CPVAs. To-date, none have studied transient behavior of such devices and in particular how the absorbers and the rotor respond to sudden changes in the excitation order and the amplitude of the fluctuating torque component.

The purpose of this work was to explore the behavior of circular-path centrifugal pendulum absorbers, as they pertain to real-world applications, specifically the automotive industry. This has been accomplished through both theoretical work and experimental testing. The following is a summary of the main contributions of this work.

5.1 Summary of Findings

- The inclusion of a general information chapter, useful for real-world applications of CPVAs.

- Outline of a new procedure for non-dimensionalizing the equations of motion, better suited to unifying results from different applications and allowing one to compare the performance from seemingly disparate systems. Results from different systems are able to be mapped into a non-dimensional parameter space for direct comparison. Previously, this was not possible with systems operating at different excitation and tuning orders.

- The choice of parameters used in simulations, approximate solutions and experiments were all guided by values from real automotive applications, with specific regard to cylinder deactivation technology.

- As predicted by the mathematics, when operating at orders well above the tuned order ($n \gg \tilde{n}$) the influence of the absorbers on the rotor dynamics is very small. Typically, absorber swing angles are an order of magnitude less than when the system is operating closer to perfect tuning. For this set of parameter values, if transients are introduced, they decay to 10% of their initial overshoot value within approximately 50 revolutions of the rotor.

- Although the results presented in Chapter 4 are not exhaustive, there is a very good indication that the amplitudes of the overshoots in the system response are within tolerable limits. For example, 50% overshoot and decay takes approximately 50 revolutions. This has been verified experimentally and through numerical simulation for cases where the absorber damping is extremely small (very conservative case). In practice the damping is likely to be larger and therefore overshoots and decay rate smaller.

- Important to note is that during the transient testing, no cases were observed where the absorber motion became unstable or "jumped" to the undesirable, large amplitude solution.

5.2 Recommendations for Future Work

Pendulum absorbers have been in use, successfully, for a significant amount of time, but there are still questions regarding various aspects of their behavior. Certain topics have been explored in this work that lead to new questions and possible directions for future work. These are:

- A more rigorous analytical study of overshoots and decay rates. The averaged equations derived in Chapter 2 could be used to explore the basins of attraction and the form of the dynamics in the vicinity of the steady-state solutions. A sudden change in a system parameter, e.g. the excitation order, n, could be viewed as a change in the initial conditions in the averaged "state-space".

- Multiple absorbers and their non-syncronous response. Although not reported here, there is experimental evidence that this can become more problematic the smaller the detuning value is, i.e. the closer n is to $\tilde{n}$. In an attempt to optimize CPVA performance it would be advantageous to be able to operate closer to perfect tuning. However, the robustness of the performance in this region would have to be fully explored.

- Experimental and theoretical work could be expanded to non-circular path absorbers.

BIBLIOGRAPHY

[1] A.S. Alsuwaiyan. *Performance, Stability, and Localization of Systems of Vibration Absorbers.* PhD thesis, Michigan State University, 1999.

[2] B.C. Carter. British patent no. 337446, 1929.

[3] C.P. Chao. *The Performance of Multiple Pendulum Vibration Absorbers Applied to Rotating Systems.* PhD thesis, Michigan State University, 1997.

[4] The Chilton and Reed Propeller Company. British patent no. 460088, 1935.

[5] Alan G. Haddow and Steven W. Shaw. Centrifugal pendulum vibration absorbers: An expermental and theoretical investigation. *Nonlinear Dynamics*, 2003.

[6] Tyler Nester. Experimental investigation of circular path centrifugal pendulum vibration absorbers. Master's thesis, Michigan State University, 2002.

[7] Peter M. Schmitz. Experimental investigation into epicycloidal centrifugal pendulum vibration absorbers. Master's thesis, Michigan State University, 2003.

[8] Peter M. Schmitz. Technical operation manual. CPVA Operation: Technical Operation Manual for Michigan State University Test Apparatus, July 2003.

[9] Steven W. Shaw. Revised circular path non-dimensionalization method. Mathematica work and hand-written notes (unpublished), September 2005.

[10] W. Ker Wilson. *Practical Solution of Torsional Vibration Problems.* Chapman and Hall Ltd, 3rd edition, 1968.